

Mid-infrared Variability-based AGN Selection using the Multi-epoch Photometric Data from WISE

SHINYU KIM ^{1,2}, MINJIN KIM ¹, SUYEON SON ³, AND LUIS C. HO ^{3,4}

¹*Department of Astronomy, Yonsei University, 50 Yonsei-ro, Seodaemun-gu, Seoul 03722, Republic of Korea*

²*Department of Astronomy and Atmospheric Sciences, Kyungpook National University, Daegu 41566, Republic of Korea*

³*Kavli Institute for Astronomy and Astrophysics, Peking University, Beijing 100871, People's Republic of China*

⁴*Department of Astronomy, School of Physics, Peking University, Beijing 100871, People's Republic of China*

ABSTRACT

We assess the systematics and efficiency of an AGN selection method based on mid-infrared (MIR) variability. To this end, we utilize various types of active and inactive galaxies from the Sloan Digital Sky Survey, matching them with multi-epoch photometric data from the NEOWISE mission. Using W1 and W2 band light curves with a ~ 10 -year baseline, we find that combining the likelihood of deviation from non-variability with the correlation coefficient between the W1 and W2 bands reliably identifies AGNs. Specifically, this MIR-based method recovers $\sim 28.2\%$ of optically selected AGNs. Applying the same technique to inactive galaxies, we identify AGN candidates at fractions ranging from 0.4 to 11.8%, indicating that MIR variability allows us to detect AGN candidates even in optically inactive hosts. While some variable sources exhibit transient-like light curves, possibly originating from tidal disruption events or supernovae, their contribution to the total variable population is less than a few percent, indicating a minimal impact on our results. Across all subsamples, the AGN fraction marginally increases with star formation activity, implying coordinated evolution between central black hole growth and star formation. Finally, the AGN fraction inferred from our method drops dramatically in classical LINERs, consistent with their low accretion rates and absence of a dusty torus.

Keywords: Galaxies (573) — Active galactic nuclei (16)

1. INTRODUCTION

The demography of active galactic nuclei (AGNs) is of great importance for understanding not only the formation and evolution of supermassive black holes (SMBHs) at the centers of massive galaxies (e.g., L. C. Ho et al. 1995, 1997a), but also the evolution of the galaxies themselves, likely through AGN-driven feedback on star formation (e.g., J. Silk & M. J. Rees 1998; J. Kormendy & L. C. Ho 2013). Therefore, identifying AGN activity within large galaxy samples is a crucial component of investigating the co-evolution of galaxies and SMBHs. To this end, previous studies have developed various methods to detect AGNs using survey datasets. Modern spectroscopic surveys, such as the Sloan Digital Sky Survey (SDSS; K. Abazajian et al. 2003), enable the classification of AGNs based on their optical spectral properties. For example, a strong UV continuum and broad

emission lines are characteristic of Type 1 AGNs (e.g. G. T. Richards et al. 2002), whereas obscured (Type 2) AGNs are primarily identified via line ratios between Balmer emissions and various forbidden lines, reflecting the harder and more intensive ionizing continuum of AGNs relative to inactive galaxies (e.g., J. A. Baldwin et al. 1981; S. Veilleux & D. E. Osterbrock 1987; L. J. Kewley et al. 2001).

Although AGN selection methods based on optical spectroscopy are widely used, they are biased against low-luminosity and highly obscured AGNs (e.g., M. Imanishi 2009; C. J. Agostino & S. Salim 2019). Because highly obscured AGNs are key to probing the AGN population, particularly in the early Universe, alternative methods are required (e.g., E. Treister & C. M. Urry 2006). One particularly effective approach utilizes mid-infrared (MIR) datasets. In typical AGNs, the dusty torus produces strong MIR emission (e.g., R. Antonucci 1993), and their MIR colors are redder than those of star-forming (SF) galaxies due to the higher dust temperatures associated with AGN activity (e.g., J. L. Don-

ley et al. 2012). Using *Spitzer* and WISE datasets, numerous studies have demonstrated that the MIR color-color diagram is efficient at detecting AGNs, especially those that are dust-obscured (e.g., M. Lacy et al. 2004; D. Stern et al. 2012; S. Mateos et al. 2012; R. J. Assef et al. 2018). Therefore, MIR color-based selection can complement conventional optical methods.

Additionally, other multiwavelength datasets, such as hard X-ray and radio, which are relatively unaffected by dust obscuration, continue to be essential for obtaining an unbiased census of the AGN population. However, all AGN identification methods suffer from their own selection biases and completeness limits. For instance, hard X-ray AGN selection is ideal for identifying obscured and unobscured AGNs with minimal systematic bias, as high-energy X-ray photons can easily penetrate dense media (e.g., K. Oh et al. 2018; M. Kim et al. 2021; M. J. Koss et al. 2022). Conversely, due to sensitivity limitations, this method is often restricted to relatively nearby sources (e.g., L. C. Ho & C. Y. Peng 2001; R. She et al. 2017). On the other hand, radio-based selection is biased toward radio-loud sources (e.g., K. I. Kellermann et al. 1989; J. Sabater et al. 2019). Since these comprise only a minor fraction of the total AGN population, this can introduce a bias into the derived statistical properties of the population (e.g., L. C. Ho & C. Y. Peng 2001; P. N. Best & T. M. Heckman 2012).

As deep MIR photometric data covering wide areas of the sky become increasingly available, the importance of MIR color-based AGN selection has been widely recognized (e.g., C. J. Lonsdale et al. 2003; E. L. Wright et al. 2010; J.-C. Mauduit et al. 2012). Due to the minimal dust extinction in this wavelength regime, it is considered one of the most effective options for obtaining an unbiased AGN census. However, contamination from starlight or warm dust within SF regions can introduce systematic effects, which often reduce the purity and completeness of the resulting samples (e.g., A. Lupi et al. 2020; W. Byun et al. 2023; J. Lyu et al. 2024). Therefore, integrating multiple selection methods is necessary to obtain a complete and unbiased view of AGN demography (R. C. Hickox & D. M. Alexander 2018; M. Siudek et al. 2025).

Alternatively, the intrinsic variability of AGNs has become a popular method for identification, as time-series photometric data have accumulated significantly through various time-domain surveys such as Stripe 82, ASAS-SN, and ZTF (Ž. Ivezić et al. 2007; C. S. Kochanek et al. 2017; E. C. Bellm et al. 2019). The majority of variability-based AGN selection relies on optical datasets (e.g., Y. Choi et al. 2014; H. Yuk et al. 2022; P. Arévalo et al. 2026), as the variability characteristics

are relatively well known (e.g., B. C. Kelly et al. 2009; S. Son et al. 2025). However, for the MIR variability, its properties are less studied compared to the optical variability (S. Kozłowski et al. 2010; S. Son et al. 2023; M. Kim et al. 2024). The MIR-based AGN selection has only been applied to a limited number of samples with specific aims (e.g., A. Pai et al. 2024; A. S. Aradhey et al. 2025). Consequently, the completeness and purity of MIR-based AGN selection have not yet been systematically validated with a sufficiently large sample. Motivated by this limitation and ongoing MIR missions, such as SPHEREx (J. J. Bock et al. 2026), this study aims to identify the optimal method for AGN selection based on MIR variability and to evaluate its efficiency and potential systematic biases. In this study, we utilize time-series datasets from the Wide-field Infrared Survey Explorer mission (WISE; E. L. Wright et al. 2010) for a diverse sample of nearby galaxies. Using these data, we validate the MIR variability-based AGN selection method. Throughout the paper, we adopt a cosmology with $H_0 = 70 \text{ km s}^{-1} \text{ Mpc}^{-1}$, $\Omega_m = 0.3$, and $\Omega_\lambda = 0.7$.

2. DATA

2.1. Sample

To examine the effectiveness of MIR variability in identifying AGNs and to investigate the physical properties of these variability-selected objects, we require a large dataset comprising various galaxy types, including both AGNs and inactive galaxies. To this end, we utilized the Max Planck Institute for Astrophysics and Johns Hopkins University (MPA–JHU) catalog (J. Brinchmann et al. 2004), derived from the SDSS Data Release 8 (SDSS DR8; H. Aihara et al. 2011). In this catalog, galaxies with strong emission lines (i.e., $S/N > 3$ for $H\beta$, $[O \text{ III}]$, $[N \text{ II}]$, and $H\alpha$) are spectroscopically classified into three subgroups [AGNs⁵, SF galaxies, and composites] based on the Baldwin, Phillips, & Terlevich (BPT) diagram (J. A. Baldwin et al. 1981) combined with the demarcation line adopted from L. J. Kewley et al. (2001); G. Kauffmann et al. (2003a). For galaxies with weak emission lines, low S/N subtypes are defined based on the line ratios. For instance, the low-ionization nuclear emission-line regions (LINERs) are defined as galaxies with $[N \text{ II}]/H\alpha > 0.6$, where other emission lines exhibit low S/N (< 3). The targets with an $H\alpha$ S/N larger than 2, which have not been classified as AGN or composites, are considered low S/N SF. Finally, galaxies with no detectable emission lines or that cannot be

⁵ The majority of the AGN sample are type 2 objects, lacking broad emission lines.

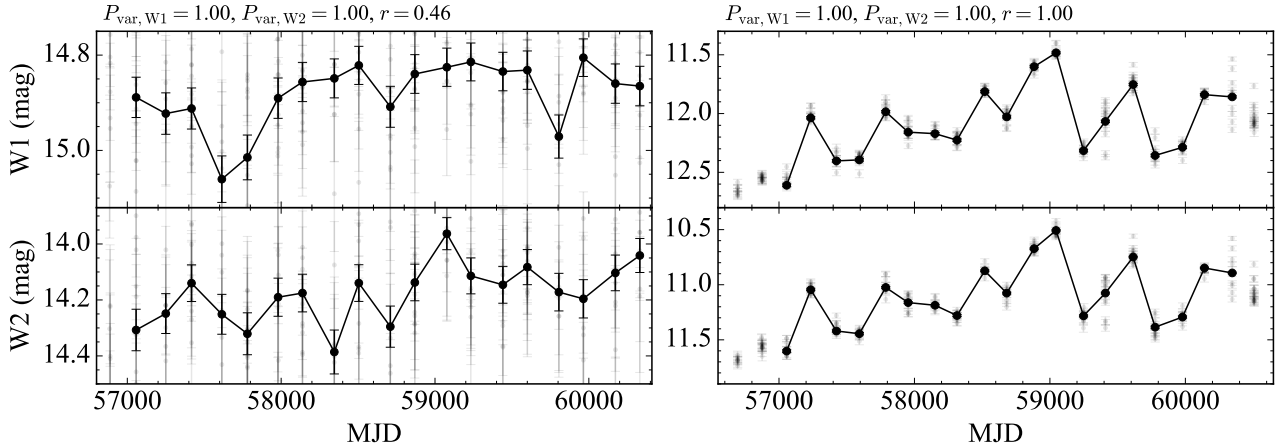


Figure 1. Two examples of light curves from our AGN sample. The faint dots denote the original data prior to binning, while the large circles represent the binned data. Due to the artificial offset between AllWISE and NEOWISE, we show only the photometric data from NEOWISE. The top and bottom panels correspond to the W1 and W2 magnitudes, respectively. The left panel shows an example that fulfills the Group 1 criteria but has $r < 0.75$, whereas the right panel shows an example that satisfies the Group 2 criteria.

classified using the BPT diagram are classified as normal galaxies. The MPA–JHU catalog includes a total of ~ 1.5 million galaxies, consisting of 1.8%, 14.6%, 59.1%, 3.5%, 5.3%, and 15.7% classified as AGN, SF, normal, composite, LINER, and low-S/N SF, respectively. It is worthwhile to note that the classification of ‘LINER’ adopted in the MPA–JHU catalog differs slightly from the conventional definition. The classical LINERs are defined as having $[\text{O III}]/\text{H}\beta < 3$ and $[\text{N II}]/\text{H}\alpha \geq 0.6$ (e.g., L. C. Ho et al. 1997b).

We note that duplicate measurements exist in the MPA–JHU catalog. We treat sources within 2 arcsec as duplicates and discard them from the sample. Occasionally, a single target is assigned to multiple subsamples and is therefore excluded from further analysis. This removes $\sim 11.6\%$ of the initial galaxy sample, resulting in a total of ~ 1.3 million galaxies. The majority of emission-line galaxies exhibit redshifts below 0.4, as the $\text{H}\beta$ and $[\text{O III}]$ emission lines used for the classification are covered by the SDSS spectral range only up to this redshift. In contrast, normal galaxies span a broader redshift distribution, extending to $z \approx 0.7$, which may introduce a potential bias when comparing their MIR variability to that of other galaxy types.

2.2. Mid-infrared data

We compile the multi-epoch MIR data of the sample from the MPA–JHU catalog, using the AllWISE and NEOWISE data (E. L. Wright et al. 2010; A. Mainzer et al. 2011; WISE Team 2020a,b). The AllWISE and NEOWISE scan the entire sky every six months, providing a baseline of ~ 14 years. This makes the data well-suited for this study, as the MIR variability timescale

in AGNs spans from months to years in the rest-frame (e.g., S. Son et al. 2023; M. Kim et al. 2024). We initially cross-match our sample with the WISE dataset with a matching radius of 2 arcsec, considering the point spread function size (6.1 – 6.4 arcsec) of the WISE images. To ensure reliable photometry, we impose the following constraints: `qual_frame` > 0, `qi_fact` > 0, `saa_sep` > 0, `moon_masked` = ‘00’, and `cc_flags` = ‘0000’ (S. Son et al. 2022). We utilize $3.4\mu\text{m}$ and $4.6\mu\text{m}$ band data (W1 and W2, respectively) from AllWISE/NEOWISE, and $12\mu\text{m}$ band data (W3) from AllWISE.

During the survey of the WISE mission survey, typically 14 individual exposures were taken in each visit. Therefore, we bin the multi-epoch data by averaging the photometric results from multiple images using a bin size of 90 days. Upon inspecting the light curves, we occasionally detect outliers in the photometric data within a single-day baseline. These cannot be attributed to intrinsic AGN variability and are likely due to poor PSF fitting, which introduces a substantial bias.

To remove such artificial outliers, we discard photometric data with high reduced χ -square values (i.e., `w1rchi2` > 10 and `w2rchi2` > 10), as derived from the PSF fit provided by NEOWISE, prior to binning. We also note that the photometric outliers are often associated with large spatial offsets (> 1 arcsec). Therefore, we further restrict the matching radius to 1 arcsec. Even with these procedures, some photometric outliers still persist. To minimize systematic uncertainties, we utilize only bins with at least five individual measurements, discard the minimum and maximum values, and perform 3σ clipping. We carefully examine the resulting

Table 1. Percentage of MIR variability-based AGNs

Optical Class	N	Group 1	Group 2	Group 3
		(%)	(%)	(%)
(1)	(2)	(3)	(4)	(5)
AGNs	19281	34.2	28.2	9.3
Star-forming	137092	4.6	3.3	2.1
Normal	452503	2.4	1.4	1.2
Composite	39835	14.9	11.8	4.5
LINERs	60803	2.7	1.6	0.1
Low S/N SF	163346	1.2	0.4	0.2

NOTE— Col. (1): Subsample based on the optical spectral classification. Col. (2): Subsample size. Col. (3): Percentage of AGNs selected using the criteria of $P_{\text{var},W1} > 0.99$ and $P_{\text{var},W2} > 0.99$. Col. (4): Percentage of AGNs selected using the criteria of $P_{\text{var},W1} > 0.99$, $P_{\text{var},W2} > 0.99$, and $r > 0.75$. Col. (5): Percentage of AGNs selected using the criteria of $P_{\text{var},W1} > 0.99$, $P_{\text{var},W2} > 0.99$, $r > 0.75$, and $P_{\text{AGN},0.8} > 0.5$.

light curves and confirm that the majority of outliers are successfully removed with such methods.

We apply additional corrections to the photometric data to mitigate systematic uncertainties and accurately quantify the light curve variability. We addressed the gradual change in the WISE satellite detector temperature, which results from the decrease in orbital altitude and introduces systematics, by applying the zero-point correction from *S. Son et al. (2026)*. Furthermore, a photometric offset was detected between the AllWISE and NEOWISE measurements in the non-variable sources of our sample, which are selected from the normal galaxies using a criterion of $P_{\text{var}} < 0.95$ (§3.1). Since this offset could not be accurately corrected using a simple constant, we chose to omit all photometric data from the AllWISE source catalog (*A. Mainzer et al. 2014*).

Finally, having corrected the NEOWISE dataset with additional treatments, we recalculate the photometric uncertainties based on our processed dataset. For this purpose, we utilize normal galaxies, which are assumed to be non-variable. To exclude variable sources (potentially faint AGNs or transients), we discard sources judged likely to be variable based on their variability probability ($P_{\text{var}} \geq 0.95$). To this end, we compute the uncertainties by taking the average of the standard deviations from the light curves of non-variable galaxies within each magnitude bin. We then estimate the photometric uncertainties of individual measurements through interpolation.

Finally, we calculate the variability using the multi-epoch NEOWISE W1 and W2 data, requiring a minimum of 10 epochs per band. This selection results in a final usable sample size of approximately 0.9 million sources, which corresponds to $\sim 59.2\%$ of the initial sample. When considering all classes other than normal galaxies, the average fraction of excluded samples at each step was consistent, ranging from 20% to 40%. For the normal galaxies, however, a large number were removed throughout the cleaning process, resulting in an approximate total exclusion of 48%. This is likely due to their faintness in the MIR and their higher average redshift compared to the other source types.

3. METHOD

To quantify the degree of variability from the NEOWISE dataset and identify AGNs based on the MIR dataset, we adopt three independent parameters: the likelihood of deviation from non-variability (P_{var}); the correlation coefficient between W1 and W2 multi-epoch photometry; and the fraction of multi-epoch data that exhibit the AGN-like W1-W2 color (P_{AGN}), expressed as a percentage.

3.1. P_{var}

P_{var} is defined as $1 - S(\chi^2, N - 1)$, where S is the survival function, χ^2 is the reduced chi-squared statistic calculated from the observed light curve, N is the number of epochs in the light curves of the individual target. P_{var} represents the probability that the observed variance in the light curve is caused by intrinsic variability (*M. A. McLaughlin et al. 1996*). P_{var} tends to be zero if the fluctuation in the light curves is solely caused by the random measurement errors, whereas P_{var} is close to 1 if its variation is intrinsic and significantly larger than the errors. We calculate P_{var} separately at W1 and W2 bands.

While previous studies adopted a criterion of $P_{\text{var}} > 0.95$ to identify variable sources from the MIR light curves (e.g., *P. Sánchez et al. 2017*; *S. Son et al. 2022*), additional treatments applied to our photometric dataset lead us to set the selection limit in a different manner. After visually inspecting the light curves and their P_{var} values, we find that a threshold of 0.95 includes suspicious sources⁶, indicating that a more stringent constraint is required. Therefore, we adopt $P_{\text{var}} > 0.99$ for the identification of variable sources throughout this study.

⁶ Examples of light curves are shown in the Appendix.

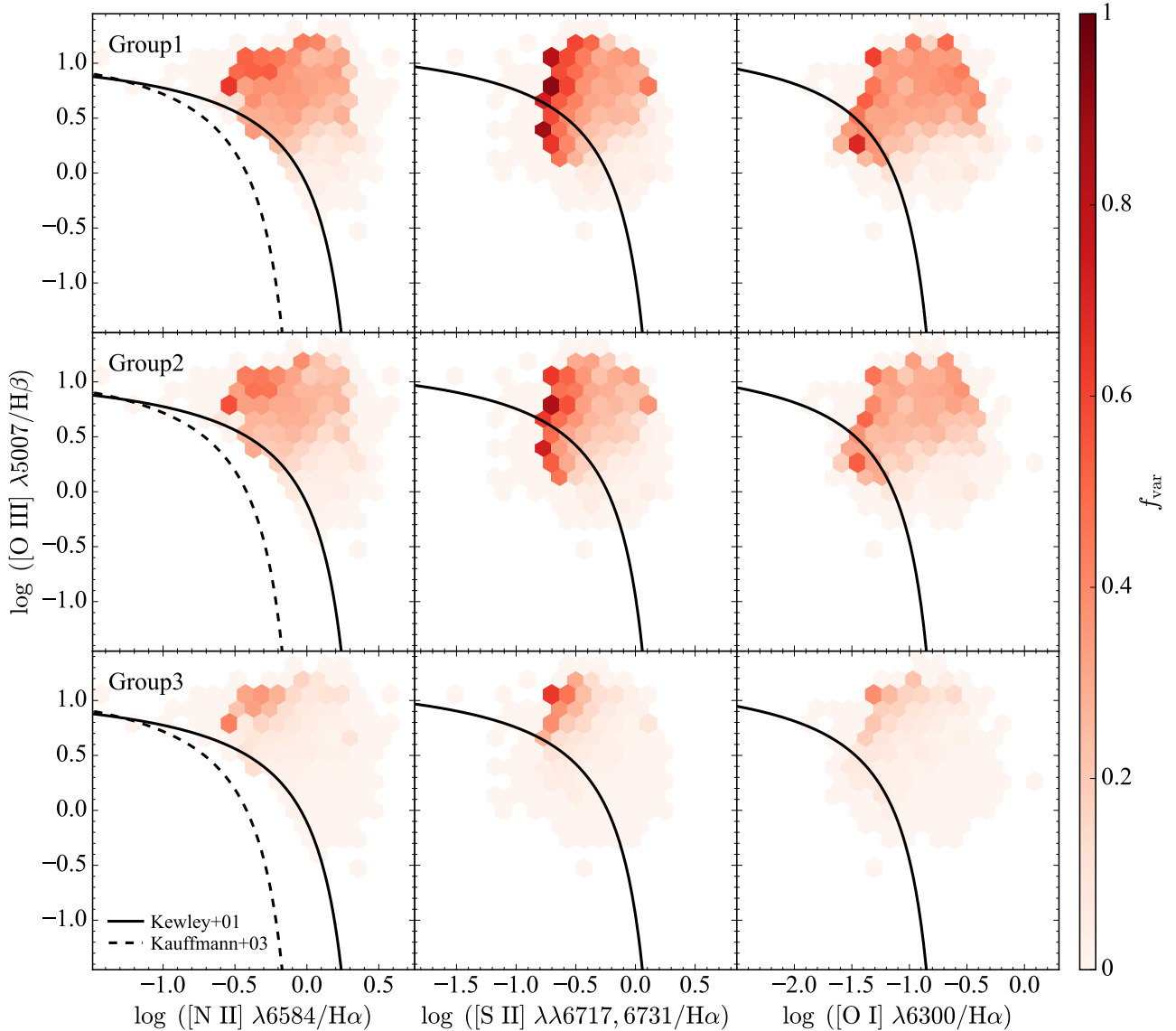


Figure 2. The BPT and VO diagrams for the optically selected AGN sample are shown. The fraction of MIR variability–selected AGNs (f_{var}) in each bin is indicated by the color maps. The original AGNs were classified as sources above the solid line adopted from L. J. Kewley et al. (2001). SF galaxies were selected below the dashed line (G. Kauffmann et al. 2003a), while sources lying between the dashed and solid lines were classified as composites. From top to bottom, MIR-based AGN classifications are presented in different categories. f_{var} is shown only in bins with more than 10 sources.

3.2. Correlation Coefficients

If the variance of the light curves is primarily caused by random errors, the photometric data for W1 and W2 are unlikely to correlate with each other. Therefore, the correlation coefficient between the W1 and W2 data can be an efficient metric for distinguishing the origin of the variability (e.g., A. S. Aradhey et al. 2025). To this end, we compute various types of cross-correlation coefficients. Prior to calculating the correlation coefficient, we match the W1 and W2 datasets so that the two light curves share the same time epochs. We use the band with the smaller number of epochs as the

reference light curve for this purpose. To synchronize the two datasets from W1 and W2, we only utilize the binned photometric data observed within ± 5 days of each other. Throughout this process, a minimum of 8 epochs is granted for our sample.

To find the best value for identifying variability, we compute four types of correlation coefficients: the Pearson correlation coefficient (r), the weighted Pearson correlation coefficient (r_w), the Spearman rank correlation coefficient (ρ_S) and Kendall’s tau (τ). For each correlation coefficient, we also calculate the corresponding p -value to evaluate its statistical significance.

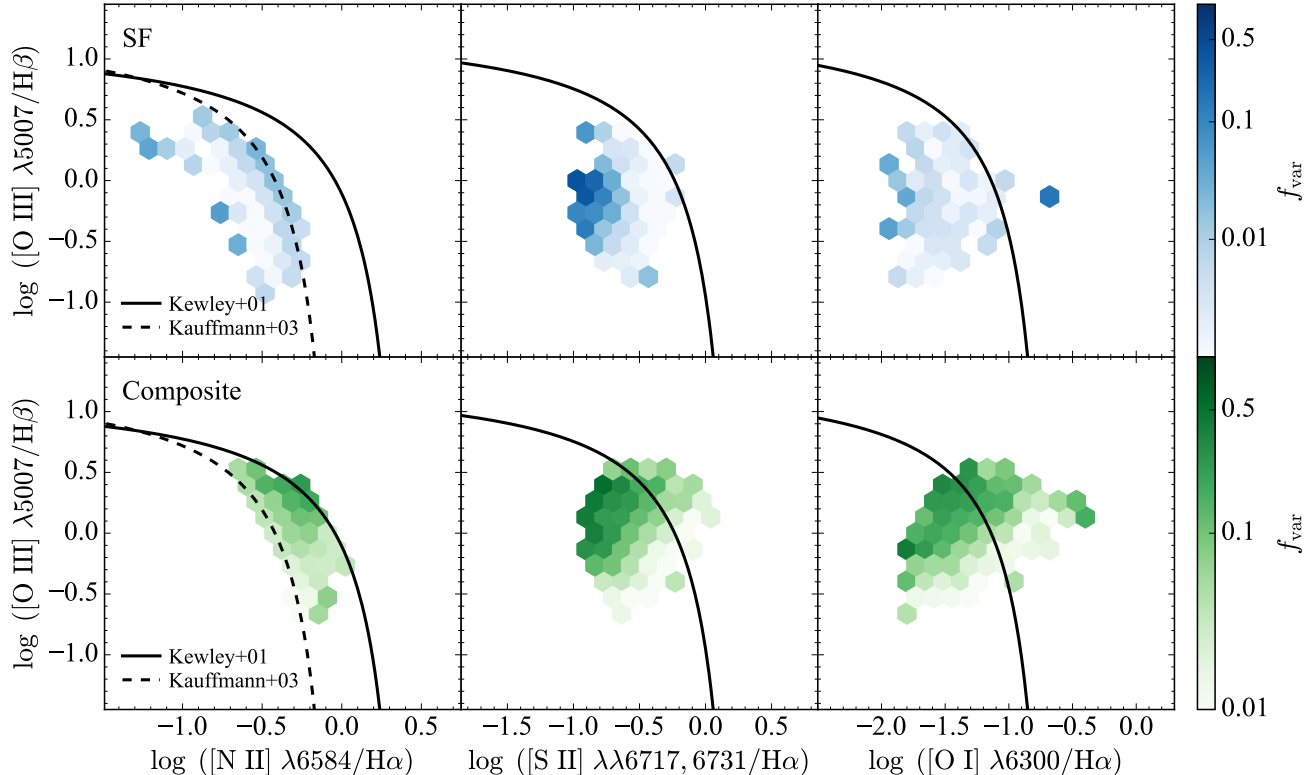


Figure 3. Same as Figure 2, except that f_{var} is shown for SF galaxies and composites. The subgroups were originally categorized in the BPT diagram (i.e., $[\text{O III}]/\text{H}\beta$ vs. $[\text{N II}]/\text{H}\alpha$)

We find that all correlation measures exhibit similar behavior, following an approximately Gaussian distribution with an extended tail at the high end. The r distribution specifically exhibits a non-Gaussian profile at $r > 0.75$, as suggested in a previous study (A. S. Aradhey et al. 2025). Consequently, we select r to identify variable sources using a threshold of 0.75. To avoid selecting statistically insignificant sources, we impose an additional criterion of $p < 0.05$.

3.3. P_{AGN}

It is well established that the higher dust temperatures in the AGN torus, compared to the relatively cold dust typically found in SF galaxies, produce distinctive MIR colors that separate AGNs from inactive galaxies (e.g., M. Lacy et al. 2004; D. Stern et al. 2005; R. J. Assef et al. 2018). Motivated by this, A. S. Aradhey et al. (2025) showed that the W1–W2 color is an effective diagnostic for identifying AGNs, complementing MIR variability, as expected from the AGN wedge in MIR color space. Following their approach, we adopt P_{AGN} , defined as the fraction of the observing period during which the matched W1–W2 color exceeds a specified threshold. We compute P_{AGN} for the threshold: $W1-W2 \geq 0.8$, which we denote as $P_{\text{AGN},0.8}$ (D. Stern

et al. 2012). However, since P_{AGN} is not directly linked to intrinsic AGN variability, we employ it as a supplementary diagnostic for validating our variability-based AGN selection method throughout this study.

4. RESULTS

4.1. Fiducial Test with AGNs

To validate the MIR variability-based AGN selection method, we first apply this method to optically selected AGNs. Using the three previously described methods, we classified galaxies into variability Groups:

Group 1: $P_{\text{var}} > 0.99$

Group 2: $P_{\text{var}} > 0.99$ & $r > 0.75$

Group 3: $P_{\text{var}} > 0.99$ & $r > 0.75$ & $P_{\text{AGN},0.8} > 0.5$

Of the entire sample of AGNs, $\sim 34\%$ exhibit variability based on the criteria of Group 1, in which P_{var} exceeds 0.99 for both bands. In general, P_{var} alone is sufficient to identify variable sources. However, instrumental failures, such as temporal fluctuations, can introduce artificial variation in the light curves. This process can result in a significant overestimation of P_{var} , leading to spurious variability detections. Additionally, the

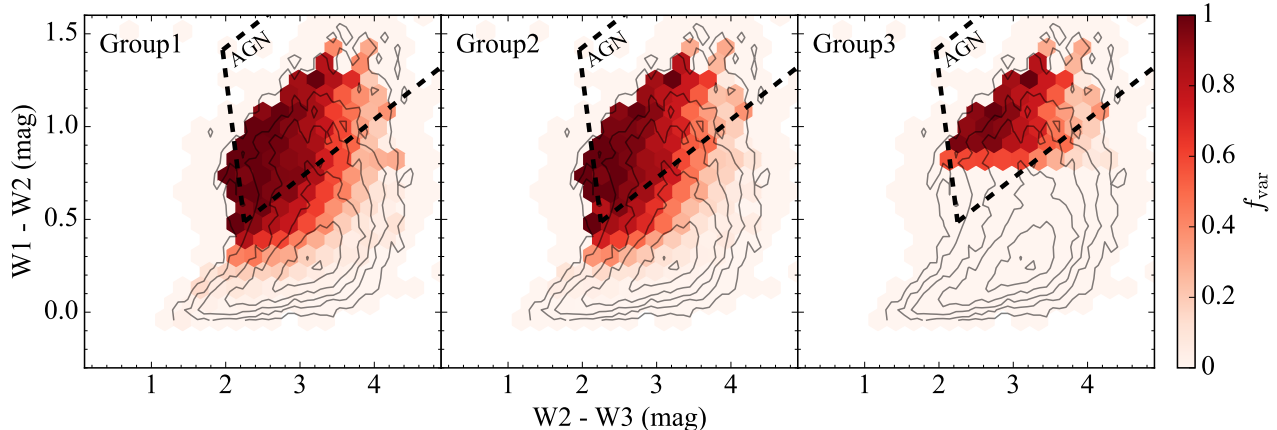


Figure 4. Distributions of MIR variability-based AGN fractions in the W1–W2 versus W2–W3 color diagram. The contours represent the density distribution of the parent sample, while the color map shows the fraction of AGN sources in each bin, categorized according to the three different criteria. The AGN fraction is only demonstrated in bins containing more than 10 sources. The thick dashed lines show the AGN wedge adopted from [S. Mateos et al. \(2012\)](#).

same impact can occur when the measurement error is underestimated. Consequently, the resulting purity of Group 1 can be low. This effect is further discussed in §5.1.

The variability fraction defined by Group 2 in the AGNs is marginally decreased to $\sim 28\%$, with an additional criterion of $r > 0.75$ from Group 1. While P_{var} is estimated in the individual band, the correlation coefficient captures simultaneous changes in both bands over the observation baseline, which is suitable for effectively detecting variance due to non-random noise. Therefore, with this additional constraint, some sources regarded as variable in Group 1, possibly due to the outliers in the photometric data, can be properly removed.

Examples of light curves are shown in Figure 1, including one object satisfying Group 1 criteria (but not Group 2) and one object classified as Group 2. An object with high P_{var} but low r indicates that variability is detected independently in each band, while the W1 and W2 bands remain uncorrelated. In such cases, the source’s variability is unlikely to originate from intrinsic physical changes. Instead, variations arise independently in each band, possibly due to random fluctuations, leading to a lower r value. We note that relaxing the constraint to $P_{\text{var}} > 0.95$ in both bands increases the Group 2 variability fraction by only 0.5%, suggesting that the P_{var} criterion is not a dominant factor in our analysis.

Notably, when applying the MIR color cut for Group 3, the MIR-selected AGN fraction dramatically decreases to $\sim 9\%$. This suggests that color-based selection may lead to the exclusion of a significant number of AGNs, particularly low- z AGNs. This trend is attributed to the fact that the MIR emission is heavily af-

ected by the stellar light from the host galaxy and dust emission from SF regions (e.g., [L. Ciesla et al. 2015](#); [S. Son et al. 2022](#)). Previous studies also demonstrated that a significant fraction of type 1 and 2 QSOs do not fulfill the MIR color criteria (i.e., $W1-W2 < 0.8$; e.g., [W. Byun et al. 2023](#)). [S. Son et al. \(2022\)](#) showed that the W1–W2 color is strongly dependent on the AGN luminosity, as the relative contribution from host galaxies is anti-correlated with the AGN luminosity. Given that our AGN sample is predominantly composed of moderate-luminosity AGNs, the MIR color cut may be inadequate for identifying such AGNs. Consequently, in this study, we identify AGN candidates based on MIR variability using the criteria of Group 2.

4.2. MIR Variability in Inactive Galaxies

We identified AGN candidates in other types of galaxies using the selection criteria (Group 2) derived from the fiducial test with optically selected AGNs. Among optically selected SF galaxies, 3.3% of sources can be categorized as AGNs, suggesting that emission lines originating from AGNs may be weak (possibly due to dust obscuration) or be overwhelmed by the emission from intense SF. Interestingly, when applying the MIR color cut, the fraction of AGNs only marginally decreases to 2.1%, implying that the detected MIR variability mostly arises from AGNs.

Conversely, the AGN fraction for composites (11.8%) is substantially larger than that for SF galaxies. This is expected, as composites are located between SF galaxies and AGNs in the BPT diagram. The connection between the MIR variability and the location at the BPT diagram is further discussed in Section 5. For galaxies with weak or no emission lines (normal, LINER, and low S/N SF galaxies), the AGN fraction derived from the

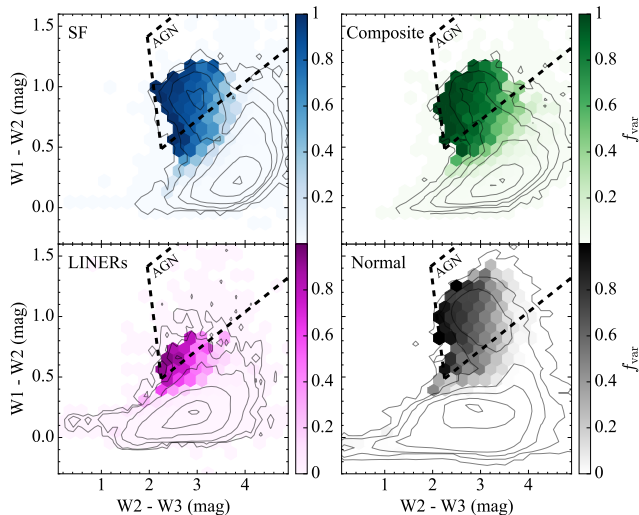


Figure 5. Same as Figure 4, for different subsamples.

MIR variability is almost negligible, ranging from 0.4 to 1.6%. Although this is not surprising given the weakness of the emission lines, it is somewhat unexpected that these three classes share a similarly low fraction, since LINERs can be powered by weak AGNs (e.g., [L. C. Ho et al. 1993](#)). It is worthwhile noting that, due to the detection limit of line emission and the limited wavelength coverage of SDSS spectra, normal galaxies exhibit higher redshift ranges compared to other subgroups. When restricting the redshift of normal galaxies to 0.4, the AGN fraction drops significantly to 0.14%. The detailed AGN fractions of subgroups based on the different selection criteria are summarized in Table 1.

5. DISCUSSION

5.1. Comparison with Other AGN Diagnostics

Conventionally, the classification of obscured AGNs has been carried out using various types of diagnostics, including line ratios of narrow emissions, MIR colors, and radio loudness (e.g., [S. Veilleux & D. E. Osterbrock 1987](#); [D. Stern et al. 2012](#); [Ž. Ivezić et al. 2002](#)). Each method has its own advantages and disadvantages. For example, the line-ratio-based method is suitable for application to large spectroscopic datasets; however, highly obscured AGNs, AGNs with prominent SF, or AGNs with weak emission lines can be missed (e.g., [C. J. Agostino & S. Salim 2019](#)). On the other hand, AGN selection based on MIR colors is effective for searching for obscured AGNs, but contamination from the host galaxies and SF regions may lead to a reduction in the completeness of the AGN sample (e.g., [M. Lacy et al. 2004](#)). To properly examine the characteristics of the MIR-variability-based method, comparisons with previous AGN selection methods are essential.

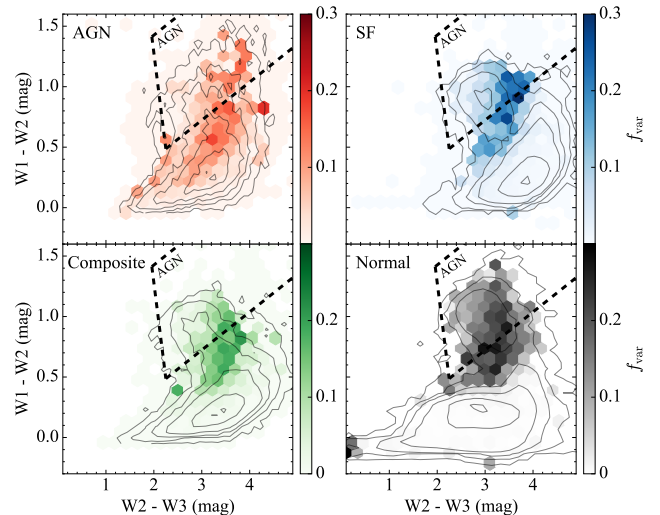


Figure 6. Same as Figure 4, for optically selected AGNs categorized as Group 1 but fulfilling Group 2 criteria.

The MPA-JHU catalog originally categorized galaxies based on their location on the BPT diagram. Therefore, it is worthwhile to compare our result with the one in that diagram. Figures 2 and 3 show the distribution of AGN fraction determined by the MIR variability in each bin. The fraction of MIR-selected AGNs is largest in the AGN location, gradually decreases in the composite region, and drops rapidly in the SF region, as expected. This clearly demonstrates the reliability of our method.

MIR color-color diagrams constructed from observations with the *Spitzer* telescope and the WISE survey have been widely employed to identify AGNs, particularly those that are dust-obscured (e.g., [M. Lacy et al. 2004](#); [D. Stern et al. 2012](#)). For our comparison, we adopt representative W1 and W2 magnitudes computed as weighted means of the multi-epoch measurements for each source, while the W3 magnitudes are taken from the AllWISE catalog. We note that a subset of the sources is not detected in the W3 band and is therefore excluded from subsequent analysis. The W3 non-detection fraction varies significantly among the different subgroups, being lowest for AGNs and highest for normal galaxies, primarily due to the intrinsic strength of MIR emission originating from warm dust.

Figure 4 shows the fraction of variable sources, categorized by different Group criteria, within the W1–W2 vs. W2–W3 diagram for optically selected AGNs. It is evident that the majority of AGNs selected based on MIR variability satisfy the AGN wedge adopted from [S. Mateos et al. \(2012\)](#), and the fraction of AGNs sharply decreases as the MIR colors deviate from this wedge. The selection based on Group 3 criteria significantly rejects genuine AGNs, thereby reducing the completeness

Table 2. Percentage of MIR variability-based AGNs within the MIR AGN Wedge

Optical Class	N	f_{wedge}	Group 1	Group 2	Group 3
(1)	(2)	(%)	(%)	(%)	(%)
AGNs	18030	15.5	37.1	42.0	90.6
Star-forming	127055	3.1	58.4	71.7	97.1
Normal	256401	3.6	74.5	88.9	98.3
Composite	37115	6.4	38.8	45.7	93.6
LINERs	51615	0.5	13.4	19.2	93.2
Low S/N SF	132856	0.3	23.4	52.8	93.6

NOTE— Col. (1): Subsample based on the optical spectral classification. Col. (2): Number of sources in the subsample with reliable photometric measurements in W1, W2, and W3. Col. (3): Percentage of sources lying within the MIR AGN wedge adopted from [S. Mateos et al. \(2012\)](#). Col. (4): Percentage of Group 1 sources satisfying the MIR AGN wedge selection criteria. Col. (5): Percentage of Group 2 sources satisfying the MIR AGN wedge selection criteria. Col. (6): Percentage of Group 3 sources satisfying the MIR AGN wedge selection criteria.

of this method. More importantly, a similar trend is observed in other galaxy types, indicating the reliability of our MIR variability-based selection method (Fig. 5). Table 2 lists the fraction of MIR variability-selected AGNs in each subsample located within the AGN wedge. To indirectly assess the purity of Group 1 criteria, we examine the fraction of variable sources that satisfy Group 1 but do not fulfill Group 2 criteria in the MIR color-color diagrams (Fig. 6). Contrary to variable sources chosen by ordinary selection criteria (i.e., Groups 1, 2, and 3), these objects are widely distributed across the color-color diagrams, suggesting that false detections may be moderate.

Furthermore, although incomplete, the radio emission can serve as an indicator of AGN activity. Therefore, it can be used to examine the reliability of our MIR-based selection. To this end, we cross-match our sample with Epoch 1 ([Y. A. Gordon et al. 2020](#)) of the Very Large Array Sky Survey (VLASS) radio data ([M. Lacy et al. 2020](#)), which provides continuum data at 2 – 4 GHz with a 1σ sensitivity of $\sim 120 \mu\text{Jy}$ over the sky area $\delta > -40^\circ$. Using a matching radius of $2''$, we find that $\approx 8.0\%$, 0.3% , 2.7% , and 2.1% of the parent sample have counterparts in the VLASS for AGNs, SF, composites, and normal galaxies, respectively. Notably, the fraction of radio detections increases by a factor of 7 – 8 (1.9%

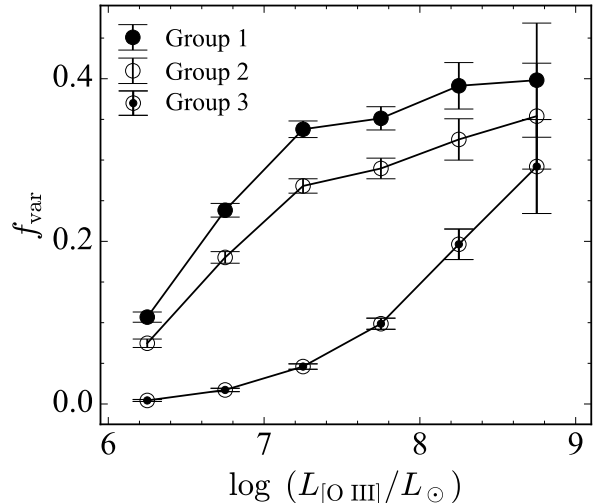


Figure 7. The fraction of MIR-based AGNs among optically selected AGNs as a function of [O III] luminosity. Subgroups based on different selection criteria are shown separately. The uncertainties are computed assuming Poisson statistics.

for SF galaxies and 16.5% for normal galaxies) for AGN candidates (Group 2). This indirectly demonstrates the reliability of our MIR-based AGN selection. However, such an increase in radio detection among AGN candidates is not observed in AGNs or composites. While the physical origin of the discrepancy between SF/normal galaxies and AGNs/composites is unclear, this may partially stem from the inverse correlation between radio loudness and Eddington ratio ([L. C. Ho 2002](#)).

5.2. Characteristics of MIR Variability-selected AGNs

Because all AGN selection techniques are subject to their own systematic effects, assessing the implications of our selection methodology is warranted. To this end, we examine how the AGN fraction depends on the physical properties of the AGNs. We first find that the fraction of MIR variability-based AGNs (f_{var}) increases with the AGN brightness, as traced by the [O III] luminosity in optically selected AGNs (Fig. 7). Furthermore, Figure 8 illustrates f_{var} as a function of redshift, BH mass (M_{BH}), and Eddington ratio (λ_{Edd}) across four distinct subgroups categorized by SDSS optical spectra. M_{BH} is estimated from the stellar mass using the M_*-M_{BH} relation (for all galaxy types) from [J. E. Greene et al. \(2020\)](#), while the bolometric luminosity (L_{bol}) is derived from the [O III] luminosity using the bolometric correction from [T. M. Heckman et al. \(2005\)](#). We assume that the entire [O III] flux originates from the AGN instead of star formation, which is a reasonable approximation for relatively massive, and hence metal-rich, host galaxies ([L. C. Ho 2005](#)). Nevertheless, the Eddington ratios for

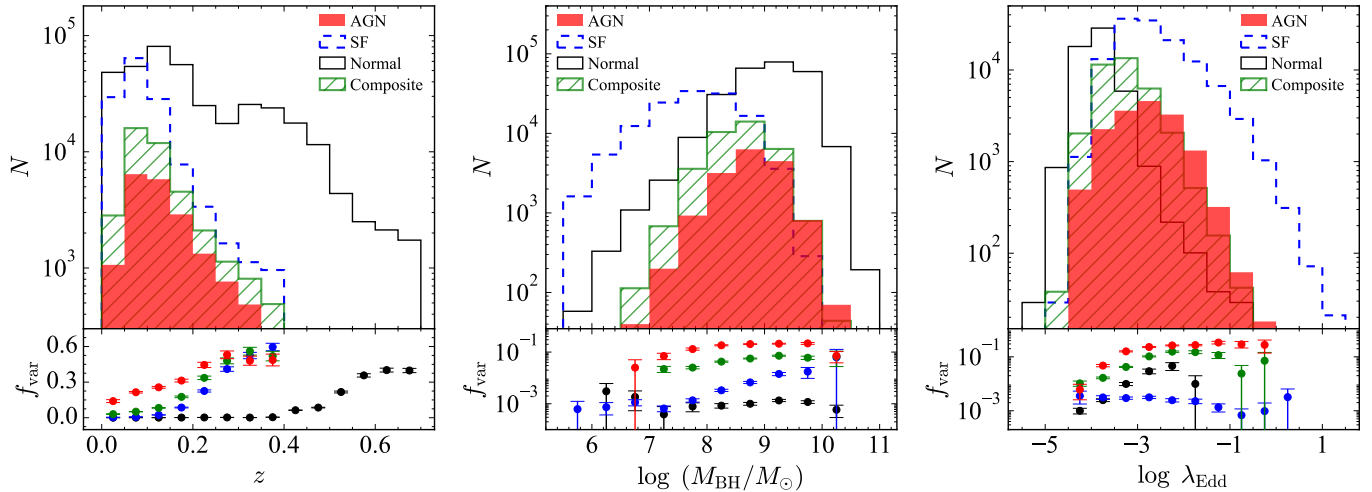


Figure 8. Distribution of the sample properties and MIR variability fractions. The top panels show the source counts for the four spectral subgroups, while the bottom panels show the corresponding fraction of MIR variable sources. From left to right, the distributions are plotted as a function of redshift (z), black hole mass (M_{BH}), and Eddington ratio (λ_{Edd}).

non-AGN subgroups should be regarded as upper limits. We note that even though we adopt other bolometric corrections, for example, those from (A. Lamastra et al. 2009), which account for extinction based on the Balmer decrement, the main result remains unchanged (see M. Kong & L. C. Ho 2018 for extensive discussion).

Notably, the fraction of variable sources increases dramatically with redshift across all subgroups. While the primary driver of this trend remains unclear, a combination of two factors (AGN luminosity and the central wavelengths of the WISE filters) may play a key role. Due to Malmquist bias, distant objects in our sample tend to be more luminous than nearby ones. Furthermore, as redshift increases, the central wavelengths of the W1 and W2 bands shift toward the peak of hot dust emission ($\sim 2-3 \mu\text{m}$; R. Mor & B. Trakhtenbrot 2011), making the observed fluxes more sensitive to MIR variability. We also find that variable sources are more common at higher BH masses. Because AGN luminosity is proportional to BH mass for a constant Eddington ratio, the observed BH mass dependence likely reflects the underlying relationship with AGN luminosity. Finally, the fraction of variable sources appears to peak at moderate Eddington ratios and decline at the extreme low end of the distribution. Interestingly, this finding is consistent with theoretical and observational studies suggesting that the torus fails to form at low Eddington ratios (e.g., M. Elitzur & I. Shlosman 2006, see §5.3 for further discussion). On the other hand, the torus may disappear at high Eddington ratios (e.g., L. C. Ho et al. 2012; M. Venanzi et al. 2020), where a decrease in f_{var} is predicted. The limited sample size of our dataset in this regime prevents us from testing this scenario.

As our method, based on MIR variability, is effective in identifying AGN candidates in dust-obscured sources and SF-dominated galaxies, it may be ideal to examine the connection between AGNs and the physical properties of galaxies, such as the star formation rate (SFR). With this motivation, we compare the locations of AGNs identified in this study in the diagram of stellar mass and SFR, which provides useful insights into the coevolution between SMBHs and their host galaxies. Note that stellar masses were calculated by combining the mass-to-light ratio at the z -band, derived from the modeling of observed spectra, and the z -band luminosity (G. Kauffmann et al. 2003b). The SFRs were estimated using the emission lines for those with detected $\text{H}\alpha$ emissions (J. Brinchmann et al. 2004). In contrast, SED fitting to the SDSS photometry was utilized to compute the SFRs of galaxies exhibiting no nebular emission lines (S. Salim et al. 2007).

Figure 9 shows the distribution of subsamples (including MIR variability-based selected AGNs) in the stellar mass-SFR diagram. SF galaxies are known to follow the relation between the star SFR and the stellar mass, which is the star formation main sequence (SFMS; K. G. Noeske et al. 2007; A. Renzini & Y.-j. Peng 2015; Y. A. Li et al. 2023). To investigate the physical connection between SF and AGN activity, it is beneficial to account for this relation. Therefore, we adopt the deviation from the SFMS, which is defined as ($\Delta\text{SFMS} \equiv \log(\text{SFR}/\text{SFR}_{\text{MS}})$), where SFR_{MS} is the SFR of the SFMS at a given stellar mass adopted from A. Saintonge et al. (2016). Figure 10 shows the relation between ΔSFMS and the fraction of AGN at a given stellar mass/SFR bin. Notably, the two quantities exhibit a

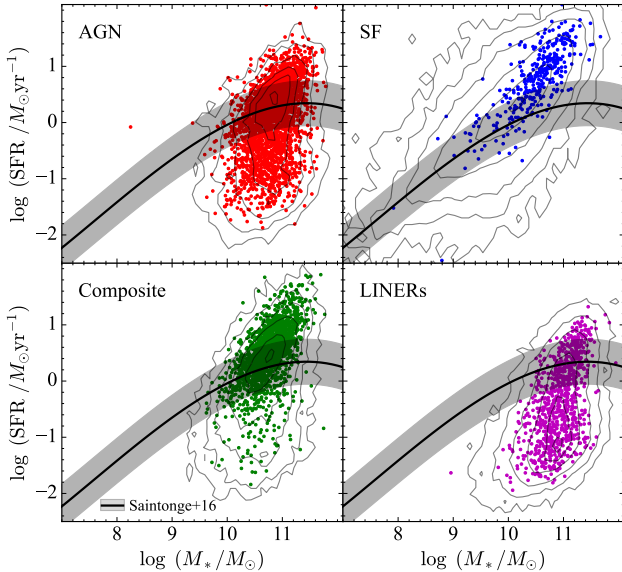


Figure 9. The relation between stellar mass and star formation rate for different subgroups. The background contours represent the parent sample in each subgroup on logarithmic scales, while the filled circles denote the MIR variability-selected AGNs based on the Group 2 criteria. The solid line indicates the star formation main sequence adopted from A. Saintonge et al. (2016). The gray-shaded region denotes the ± 0.4 dex, 1σ scatter for SFMS.

positive correlation across all subgroups, suggesting that AGN activity is synchronized with the SF. Furthermore, the observed increase of f_{var} with the AGN brightness (Fig. 7) suggests a correlation between AGN luminosity and SFR. Interestingly, this finding is consistent with previous studies based on different techniques, such as the photometric properties of host galaxies, spectral features of young stars, and the FIR-based SFR in AGNs (e.g., G. Kauffmann et al. 2003a; A. M. Diamond-Stanic & G. H. Rieke 2012; M. Kim & L. C. Ho 2019; M.-Y. Zhuang & L. C. Ho 2023). This clearly demonstrates the power of our AGN selection method based on the MIR variability, as it allows us to detect AGNs in various types of galaxies, including SF-dominated galaxies and composite systems, from a large survey dataset.

5.3. Implication for Classical LINER

The nature of LINERs, as studied through integrated, global spectroscopy, can be ambiguous because the large aperture mixes various excitation mechanisms (AGNs, shocks, and old stars). However, when properly isolated with high-resolution observations, and especially when combined with multiwavelength information, LINERs are AGNs of low Eddington ratio (L. C. Ho 2008, 2009). Here, we utilize the MIR variability of LINERs to investigate their physical properties. For clarification,

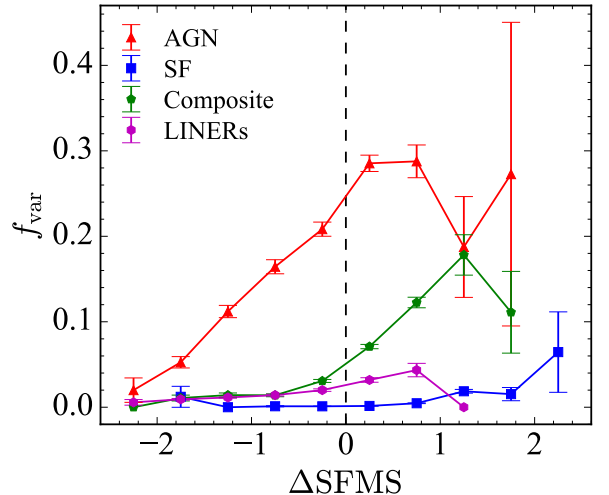


Figure 10. The fraction of MIR-selected AGNs as a function of the deviation from the SFMS (ΔSFMS) at a given stellar mass. Red, blue, green, and purple symbols represent the fractions for AGNs, SF galaxies, composites, and LINERs, respectively.

we adopt the conventional definition of LINERs, which is distinguished from the one employed in the MPA-JHU catalog. Specifically, we classify classical LINERs located below the demarcation line from L. C. Ho et al. (1997b) on the BPT diagram, resulting in 7433 objects ($\sim 46.1\%$ of optically selected AGNs). Note that LINERs from the MPA-JHU catalog are not used in the analysis due to their distinctive definition and low S/N of emission lines.

The fraction of sources associated with MIR variability significantly decreases in the classical LINERs to $\sim 11.5\%$ (Fig. 2). Furthermore, unlike the composites and SF galaxies, the classical LINERs in the MIR color-color diagram are mostly located outside the AGN wedge (Fig. 11). The fraction of sources within the AGN wedge is even smaller than that of normal galaxies. This result may suggest that the classical LINERs possess low-luminosity AGNs, where their MIR color is mostly dominated by the stellar light, or that they have a non-AGN origin (L. C. Ho et al. 1993; L. C. Ho 2008, 2009). However, these explanations are insufficient to account for the extremely low MIR variability and the redder MIR colors observed in these galaxies compared to other inactive galaxies (see also L. C. Ho 2009).

Instead, they may be low-luminosity AGNs that lack the dusty torus, unlike ordinary luminous AGNs. This is the prediction from the disk-wind driven torus formation, where the outflow from the accretion disk drives the formation of the dusty torus and dense gas clouds in the broad line regions (e.g., M. Elitzur & I. Shlosman

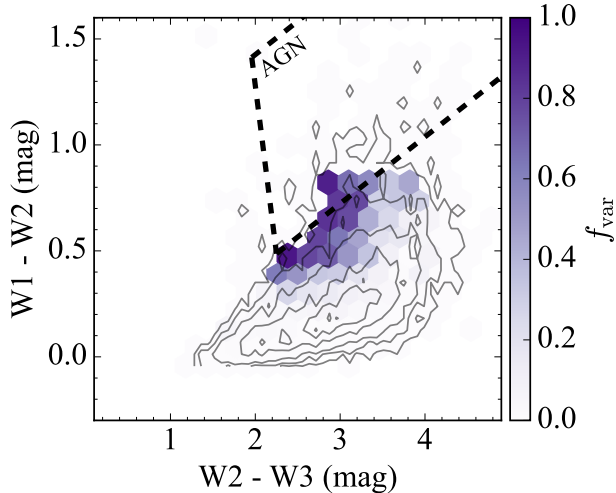


Figure 11. Same as Figure 4, for classic LINERs classified using the definition from L. C. Ho et al. (1997b).

2006; M. Elitzur & L. C. Ho 2009; K. Wada 2012). In this model, the broad line region and torus may disappear in low-luminosity AGNs because the outflow cannot be sustained under these conditions. Notably, this prediction is adequate to explain the extremely low MIR luminosity of the classical LINERs (see also L. C. Ho 1999, 2008, 2009).

5.4. Caveat

MIR variability can arise from sources other than AGNs, including rare events such as supernovae (SNe) and tidal disruption events (TDEs). Therefore, their contribution should be addressed properly. For TDEs, their low incident rate, estimated between 10^{-5} and 10^{-4} yr $^{-1}$ (e.g., N. C. Stone & B. D. Metzger 2016), makes them infrequent contaminants. Their rate is further suppressed for the black hole masses in our sample, as the TDE rate peaks around $M_{\text{BH}} \sim 10^{6.5} M_{\odot}$ and declines at higher masses. Additionally, the dust obscuring TDEs is minimal, with a covering factor of only up to 1% (e.g. N. Jiang et al. 2021). Therefore, given the ~ 10 -year observational span of NEOWISE, the likelihood of TDE contamination is considered negligible.

The incident rate for SNe is significantly higher than for TDEs, and unlike TDEs, SNe can occur in the galactic outskirts. Furthermore, SNe are categorized into various types, with differing energy outputs and rates among the subgroups (e.g., W. Li et al. 2011). Moreover, the dust formation mechanism and covering factor in SNe remain debated (e.g., T. Szalai et al. 2019). Given these combined factors, quantifying the potential for SNe contamination is difficult. For this reason, we visually inspect the observed light curves of 1000 randomly selected SF galaxies that exhibit MIR variability

according to the Group 2 criteria. We select SF galaxies because they are primarily affected by SNe, whose rate is known to be proportional to SF rates (e.g., F. Mannucci et al. 2005). Of these, we identify 11 transient-like light curves (i.e., a monotonic decrease of brightness occasionally followed by a sudden increase). Examples of such light curves are shown in Figure 12. This result suggests that the effect of SNe is also minimal.

6. CONCLUSION

To investigate an AGN-selection technique based on MIR variability, we use a sample of low-redshift galaxies from the MPA-JHU catalog, including both active and inactive systems. We cross-match this sample with NEOWISE and extract nearly a decade of MIR time-series photometry, obtained at a typical cadence of ~ 6 months. After performing a careful calibration to remove spurious measurements, we construct high-quality MIR light curves for all matched sources. Using this dataset, we identify AGN candidates based on three variability-diagnostic parameters: (1) the likelihood of deviation from a non-variable light curve, P_{var} ; (2) the correlation coefficient between the W1 and W2 multi-epoch light curves, r ; and (3) the fraction of epochs exhibiting the red W1–W2 color characteristic of known AGNs, P_{AGN} . From this analysis, we draw the following conclusions:

- From a fiducial test using optically selected AGNs, we find that AGNs can be reliably identified by applying two criteria: (1) $P_{\text{var},W1} > 0.99$ and $P_{\text{var},W2} > 0.99$ and (2) $r > 0.75$. With these selection requirements, we successfully identify AGNs for $\sim 28\%$ of the optically selected AGN sample.
- Applying conventional MIR color-based selection criteria reduces the AGN recovery fraction from $\sim 28\%$ to $\sim 9\%$, indicating that MIR color selection alone is inefficient for identifying AGNs whose MIR emission is strongly contaminated by stellar light or SF regions.
- By applying the same criteria, we identify AGN candidates for $\sim 12\%$, $\sim 3\%$, and $\sim 1\%$ of composites, SF galaxies, and normal galaxies, respectively. This suggests that AGNs can be missed when using only optical emission lines for classification.
- Comparisons with other AGN diagnostics show that our MIR variability-based selection is broadly consistent with alternative methods, although non-negligible discrepancies remain among different AGN indicators. These results suggest that

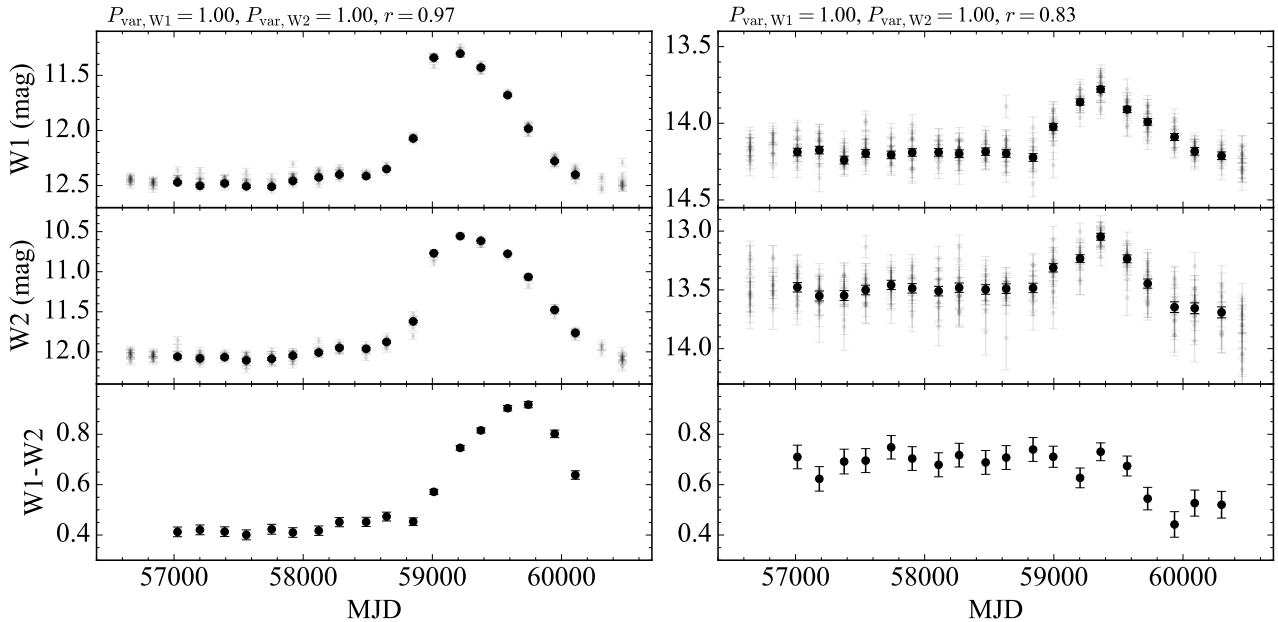


Figure 12. Two examples of light curves showing the transient-like phenomena. The top and middle panels are the same as in Figure 1, while the bottom panels represent the W1–W2 color.

our approach is most effective for luminous AGNs and for identifying AGN candidates in star formation–dominated systems, while its overall completeness remains relatively low.

- By comparing the AGN fraction (f_{var}) derived from our MIR-based method with the offset from the SFMS (ΔSFMS) in the $M_* - \text{SFR}$ plane, we find that f_{var} increases with increasing of ΔSFMS . This trend suggests that AGN activity is closely connected to SF, providing evidence for the co-evolution of SMBHs and their host galaxies.
- For classical LINERs, the MIR variability-based AGN fraction is significantly lower than that of classical AGNs. This result is consistent with the fact that LINERs host predominantly low-luminosity AGNs or may lack a substantial dusty torus as a consequence of their low accretion luminosities.
- The MIR variability can also be produced by other transient phenomena, such as SNe or TDEs. However, their occurrence rates are expected to be neg-

ligible and therefore have little impact on the conclusions of this study.

ACKNOWLEDGMENTS

We are grateful to the anonymous referee for valuable comments and suggestions, which greatly improved our manuscript. LCH was supported by the National Science Foundation of China (12233001) and the China Manned Space Program (CMS-CSST-2025-A09). This work was supported by the National Research Foundation of Korea (NRF) grant funded by the Korean government (MSIT) (Nos. RS-2024-00347548 and RS-2025-16066624) and the Yonsei University Research Fund of 2025 (2025-22-0402).

Facilities: WISE, NEOWISE

Software: Astropy (Astropy Collaboration et al. 2013, 2018, 2022), SciPy (P. Virtanen et al. 2020), NumPy (C. R. Harris et al. 2020), Matplotlib (J. D. Hunter 2007), scikit-learn (F. Pedregosa et al. 2011), pandas (T. pandas development team 2020), NetworkX (A. A. Hagberg et al. 2008)

REFERENCES

Abazajian, K., Adelman-McCarthy, J. K., Agüeros, M. A., et al. 2003, *AJ*, 126, 2081, doi: [10.1086/378165](https://doi.org/10.1086/378165)

Agostino, C. J., & Salim, S. 2019, *ApJ*, 876, 12, doi: [10.3847/1538-4357/ab1094](https://doi.org/10.3847/1538-4357/ab1094)

- Aihara, H., Allende Prieto, C., An, D., et al. 2011, *ApJS*, 193, 29, doi: [10.1088/0067-0049/193/2/29](https://doi.org/10.1088/0067-0049/193/2/29)
- Antonucci, R. 1993, *ARA&A*, 31, 473, doi: [10.1146/annurev.aa.31.090193.002353](https://doi.org/10.1146/annurev.aa.31.090193.002353)
- Aradhey, A. S., Constantin, A., Vogeley, M. S., & Douglass, K. A. 2025, *ApJ*, 991, 52, doi: [10.3847/1538-4357/adeca1](https://doi.org/10.3847/1538-4357/adeca1)
- Arévalo, P., Sánchez-Sáez, P., Sotomayor, B., et al. 2026, *A&A*, 705, A247, doi: [10.1051/0004-6361/202556258](https://doi.org/10.1051/0004-6361/202556258)
- Assef, R. J., Stern, D., Noirot, G., et al. 2018, *ApJS*, 234, 23, doi: [10.3847/1538-4365/aaa00a](https://doi.org/10.3847/1538-4365/aaa00a)
- Astropy Collaboration, Robitaille, T. P., Tollerud, E. J., et al. 2013, *A&A*, 558, A33, doi: [10.1051/0004-6361/201322068](https://doi.org/10.1051/0004-6361/201322068)
- Astropy Collaboration, Price-Whelan, A. M., Sipőcz, B. M., et al. 2018, *AJ*, 156, 123, doi: [10.3847/1538-3881/aabc4f](https://doi.org/10.3847/1538-3881/aabc4f)
- Astropy Collaboration, Price-Whelan, A. M., Lim, P. L., et al. 2022, *ApJ*, 935, 167, doi: [10.3847/1538-4357/ac7c74](https://doi.org/10.3847/1538-4357/ac7c74)
- Baldwin, J. A., Phillips, M. M., & Terlevich, R. 1981, *PASP*, 93, 5, doi: [10.1086/130766](https://doi.org/10.1086/130766)
- Bellm, E. C., Kulkarni, S. R., Graham, M. J., et al. 2019, *PASP*, 131, 018002, doi: [10.1088/1538-3873/aaecbe](https://doi.org/10.1088/1538-3873/aaecbe)
- Best, P. N., & Heckman, T. M. 2012, *MNRAS*, 421, 1569, doi: [10.1111/j.1365-2966.2012.20414.x](https://doi.org/10.1111/j.1365-2966.2012.20414.x)
- Bock, J. J., Aboobaker, A. M., Adamo, J., et al. 2026, arXiv e-prints, arXiv:2511.02985, doi: [10.48550/arXiv.2511.02985](https://doi.org/10.48550/arXiv.2511.02985)
- Brinchmann, J., Charlot, S., White, S. D. M., et al. 2004, *MNRAS*, 351, 1151, doi: [10.1111/j.1365-2966.2004.07881.x](https://doi.org/10.1111/j.1365-2966.2004.07881.x)
- Byun, W., Kim, M., Sheen, Y.-K., et al. 2023, *ApJS*, 268, 57, doi: [10.3847/1538-4365/acebe4](https://doi.org/10.3847/1538-4365/acebe4)
- Choi, Y., Gibson, R. R., Becker, A. C., et al. 2014, *ApJ*, 782, 37, doi: [10.1088/0004-637X/782/1/37](https://doi.org/10.1088/0004-637X/782/1/37)
- Ciesla, L., Charmandaris, V., Georgakakis, A., et al. 2015, *A&A*, 576, A10, doi: [10.1051/0004-6361/201425252](https://doi.org/10.1051/0004-6361/201425252)
- Diamond-Stanic, A. M., & Rieke, G. H. 2012, *ApJ*, 746, 168, doi: [10.1088/0004-637X/746/2/168](https://doi.org/10.1088/0004-637X/746/2/168)
- Donley, J. L., Koekemoer, A. M., Brusa, M., et al. 2012, *ApJ*, 748, 142, doi: [10.1088/0004-637X/748/2/142](https://doi.org/10.1088/0004-637X/748/2/142)
- Elitzur, M., & Ho, L. C. 2009, *ApJL*, 701, L91, doi: [10.1088/0004-637X/701/2/L91](https://doi.org/10.1088/0004-637X/701/2/L91)
- Elitzur, M., & Shlosman, I. 2006, *ApJL*, 648, L101, doi: [10.1086/508158](https://doi.org/10.1086/508158)
- Gordon, Y. A., Boyce, M. M., O’Dea, C. P., et al. 2020, *Research Notes of the American Astronomical Society*, 4, 175, doi: [10.3847/2515-5172/abbe23](https://doi.org/10.3847/2515-5172/abbe23)
- Greene, J. E., Strader, J., & Ho, L. C. 2020, *ARA&A*, 58, 257, doi: [10.1146/annurev-astro-032620-021835](https://doi.org/10.1146/annurev-astro-032620-021835)
- Hagberg, A. A., Schult, D. A., & Swart, P. J. 2008, in *Proceedings of the 7th Python in Science Conference*, ed. G. Varoquaux, T. Vaught, & J. Millman, Pasadena, CA USA, 11 – 15
- Harris, C. R., Millman, K. J., van der Walt, S. J., et al. 2020, *Nature*, 585, 357, doi: [10.1038/s41586-020-2649-2](https://doi.org/10.1038/s41586-020-2649-2)
- Heckman, T. M., Ptak, A., Hornschemeier, A., & Kauffmann, G. 2005, *ApJ*, 634, 161, doi: [10.1086/491665](https://doi.org/10.1086/491665)
- Hickox, R. C., & Alexander, D. M. 2018, *ARA&A*, 56, 625, doi: [10.1146/annurev-astro-081817-051803](https://doi.org/10.1146/annurev-astro-081817-051803)
- Ho, L. C. 1999, *ApJ*, 516, 672, doi: [10.1086/307137](https://doi.org/10.1086/307137)
- Ho, L. C. 2002, *ApJ*, 564, 120, doi: [10.1086/324399](https://doi.org/10.1086/324399)
- Ho, L. C. 2005, *ApJ*, 629, 680, doi: [10.1086/431643](https://doi.org/10.1086/431643)
- Ho, L. C. 2008, *ARA&A*, 46, 475, doi: [10.1146/annurev.astro.45.051806.110546](https://doi.org/10.1146/annurev.astro.45.051806.110546)
- Ho, L. C. 2009, *ApJ*, 699, 626, doi: [10.1088/0004-637X/699/1/626](https://doi.org/10.1088/0004-637X/699/1/626)
- Ho, L. C., Filippenko, A. V., & Sargent, W. L. 1995, *ApJS*, 98, 477, doi: [10.1086/192170](https://doi.org/10.1086/192170)
- Ho, L. C., Filippenko, A. V., & Sargent, W. L. W. 1993, *ApJ*, 417, 63, doi: [10.1086/173291](https://doi.org/10.1086/173291)
- Ho, L. C., Filippenko, A. V., & Sargent, W. L. W. 1997a, *ApJ*, 487, 568, doi: [10.1086/304638](https://doi.org/10.1086/304638)
- Ho, L. C., Filippenko, A. V., & Sargent, W. L. W. 1997b, *ApJS*, 112, 315, doi: [10.1086/313041](https://doi.org/10.1086/313041)
- Ho, L. C., Kim, M., & Terashima, Y. 2012, *ApJL*, 759, L16, doi: [10.1088/2041-8205/759/1/L16](https://doi.org/10.1088/2041-8205/759/1/L16)
- Ho, L. C., & Peng, C. Y. 2001, *ApJ*, 555, 650, doi: [10.1086/321524](https://doi.org/10.1086/321524)
- Hunter, J. D. 2007, *Computing in Science & Engineering*, 9, 90, doi: [10.1109/MCSE.2007.55](https://doi.org/10.1109/MCSE.2007.55)
- Imanishi, M. 2009, *ApJ*, 694, 751, doi: [10.1088/0004-637X/694/2/751](https://doi.org/10.1088/0004-637X/694/2/751)
- Ivezić, Ž., Menou, K., Knapp, G. R., et al. 2002, *AJ*, 124, 2364, doi: [10.1086/344069](https://doi.org/10.1086/344069)
- Ivezić, Ž., Smith, J. A., Miknaitis, G., et al. 2007, *AJ*, 134, 973, doi: [10.1086/519976](https://doi.org/10.1086/519976)
- Jiang, N., Wang, T., Hu, X., et al. 2021, *ApJ*, 911, 31, doi: [10.3847/1538-4357/abe772](https://doi.org/10.3847/1538-4357/abe772)
- Kauffmann, G., Heckman, T. M., Tremonti, C., et al. 2003a, *MNRAS*, 346, 1055, doi: [10.1111/j.1365-2966.2003.07154.x](https://doi.org/10.1111/j.1365-2966.2003.07154.x)
- Kauffmann, G., Heckman, T. M., White, S. D. M., et al. 2003b, *MNRAS*, 341, 33, doi: [10.1046/j.1365-8711.2003.06291.x](https://doi.org/10.1046/j.1365-8711.2003.06291.x)
- Kellermann, K. I., Sramek, R., Schmidt, M., Shaffer, D. B., & Green, R. 1989, *AJ*, 98, 1195, doi: [10.1086/115207](https://doi.org/10.1086/115207)
- Kelly, B. C., Bechtold, J., & Siemiginowska, A. 2009, *ApJ*, 698, 895, doi: [10.1088/0004-637X/698/1/895](https://doi.org/10.1088/0004-637X/698/1/895)

- Kewley, L. J., Dopita, M. A., Sutherland, R. S., Heisler, C. A., & Trevena, J. 2001, *ApJ*, 556, 121, doi: [10.1086/321545](https://doi.org/10.1086/321545)
- Kim, M., Barth, A. J., Ho, L. C., & Son, S. 2021, *ApJS*, 256, 40, doi: [10.3847/1538-4365/ac133e](https://doi.org/10.3847/1538-4365/ac133e)
- Kim, M., & Ho, L. C. 2019, *ApJ*, 876, 35, doi: [10.3847/1538-4357/ab11cf](https://doi.org/10.3847/1538-4357/ab11cf)
- Kim, M., Son, S., & Ho, L. C. 2024, *A&A*, 689, A27, doi: [10.1051/0004-6361/202450413](https://doi.org/10.1051/0004-6361/202450413)
- Kochanek, C. S., Shappee, B. J., Stanek, K. Z., et al. 2017, *PASP*, 129, 104502, doi: [10.1088/1538-3873/aa80d9](https://doi.org/10.1088/1538-3873/aa80d9)
- Kong, M., & Ho, L. C. 2018, *ApJ*, 859, 116, doi: [10.3847/1538-4357/aabe2a](https://doi.org/10.3847/1538-4357/aabe2a)
- Kormendy, J., & Ho, L. C. 2013, *ARA&A*, 51, 511, doi: [10.1146/annurev-astro-082708-101811](https://doi.org/10.1146/annurev-astro-082708-101811)
- Koss, M. J., Trakhtenbrot, B., Ricci, C., et al. 2022, *ApJS*, 261, 1, doi: [10.3847/1538-4365/ac6c8f](https://doi.org/10.3847/1538-4365/ac6c8f)
- Kozłowski, S., Kochanek, C. S., Stern, D., et al. 2010, *ApJ*, 716, 530, doi: [10.1088/0004-637X/716/1/530](https://doi.org/10.1088/0004-637X/716/1/530)
- Lacy, M., Storrie-Lombardi, L. J., Sajina, A., et al. 2004, *ApJS*, 154, 166, doi: [10.1086/422816](https://doi.org/10.1086/422816)
- Lacy, M., Baum, S. A., Chandler, C. J., et al. 2020, *PASP*, 132, 035001, doi: [10.1088/1538-3873/ab63eb](https://doi.org/10.1088/1538-3873/ab63eb)
- Lamastra, A., Bianchi, S., Matt, G., et al. 2009, *A&A*, 504, 73, doi: [10.1051/0004-6361/200912023](https://doi.org/10.1051/0004-6361/200912023)
- Li, W., Leaman, J., Chornock, R., et al. 2011, *MNRAS*, 412, 1441, doi: [10.1111/j.1365-2966.2011.18160.x](https://doi.org/10.1111/j.1365-2966.2011.18160.x)
- Li, Y. A., Ho, L. C., Shangguan, J., Zhuang, M.-Y., & Li, R. 2023, *ApJS*, 267, 17, doi: [10.3847/1538-4365/acd4b5](https://doi.org/10.3847/1538-4365/acd4b5)
- Lonsdale, C. J., Smith, H. E., Rowan-Robinson, M., et al. 2003, *PASP*, 115, 897, doi: [10.1086/376850](https://doi.org/10.1086/376850)
- Lupi, A., Sbarrato, T., & Carniani, S. 2020, *MNRAS*, 492, 2528, doi: [10.1093/mnras/stz3636](https://doi.org/10.1093/mnras/stz3636)
- Lyu, J., Alberts, S., Rieke, G. H., et al. 2024, *ApJ*, 966, 229, doi: [10.3847/1538-4357/ad3643](https://doi.org/10.3847/1538-4357/ad3643)
- Mainzer, A., Bauer, J., Grav, T., et al. 2011, *ApJ*, 731, 53, doi: [10.1088/0004-637X/731/1/53](https://doi.org/10.1088/0004-637X/731/1/53)
- Mainzer, A., Bauer, J., Cutri, R. M., et al. 2014, *ApJ*, 792, 30, doi: [10.1088/0004-637X/792/1/30](https://doi.org/10.1088/0004-637X/792/1/30)
- Mannucci, F., Della Valle, M., Panagia, N., et al. 2005, *A&A*, 433, 807, doi: [10.1051/0004-6361:20041411](https://doi.org/10.1051/0004-6361:20041411)
- Mateos, S., Alonso-Herrero, A., Carrera, F. J., et al. 2012, *MNRAS*, 426, 3271, doi: [10.1111/j.1365-2966.2012.21843.x](https://doi.org/10.1111/j.1365-2966.2012.21843.x)
- Mauduit, J.-C., Lacy, M., Farrah, D., et al. 2012, *PASP*, 124, 714, doi: [10.1086/666945](https://doi.org/10.1086/666945)
- McLaughlin, M. A., Mattox, J. R., Cordes, J. M., & Thompson, D. J. 1996, *ApJ*, 473, 763, doi: [10.1086/178188](https://doi.org/10.1086/178188)
- Mor, R., & Trakhtenbrot, B. 2011, *ApJL*, 737, L36, doi: [10.1088/2041-8205/737/2/L36](https://doi.org/10.1088/2041-8205/737/2/L36)
- Noeske, K. G., Weiner, B. J., Faber, S. M., et al. 2007, *ApJL*, 660, L43, doi: [10.1086/517926](https://doi.org/10.1086/517926)
- Oh, K., Koss, M., Markwardt, C. B., et al. 2018, *ApJS*, 235, 4, doi: [10.3847/1538-4365/aaa7fd](https://doi.org/10.3847/1538-4365/aaa7fd)
- Pai, A., Blanton, M. R., & Moustakas, J. 2024, *ApJ*, 977, 102, doi: [10.3847/1538-4357/ad89b8](https://doi.org/10.3847/1538-4357/ad89b8)
- pandas development team, T. 2020, *pandas-dev/pandas: Pandas*, latest Zenodo, doi: [10.5281/zenodo.3509134](https://doi.org/10.5281/zenodo.3509134)
- Pedregosa, F., Varoquaux, G., Gramfort, A., et al. 2011, *Journal of Machine Learning Research*, 12, 2825
- Renzini, A., & Peng, Y.-j. 2015, *ApJL*, 801, L29, doi: [10.1088/2041-8205/801/2/L29](https://doi.org/10.1088/2041-8205/801/2/L29)
- Richards, G. T., Fan, X., Newberg, H. J., et al. 2002, *AJ*, 123, 2945, doi: [10.1086/340187](https://doi.org/10.1086/340187)
- Sabater, J., Best, P. N., Hardcastle, M. J., et al. 2019, *A&A*, 622, A17, doi: [10.1051/0004-6361/201833883](https://doi.org/10.1051/0004-6361/201833883)
- Saintonge, A., Catinella, B., Cortese, L., et al. 2016, *MNRAS*, 462, 1749, doi: [10.1093/mnras/stw1715](https://doi.org/10.1093/mnras/stw1715)
- Salim, S., Rich, R. M., Charlot, S., et al. 2007, *ApJS*, 173, 267, doi: [10.1086/519218](https://doi.org/10.1086/519218)
- Sánchez, P., Lira, P., Cartier, R., et al. 2017, *ApJ*, 849, 110, doi: [10.3847/1538-4357/aa9188](https://doi.org/10.3847/1538-4357/aa9188)
- She, R., Ho, L. C., & Feng, H. 2017, *ApJ*, 835, 223, doi: [10.3847/1538-4357/835/2/223](https://doi.org/10.3847/1538-4357/835/2/223)
- Silk, J., & Rees, M. J. 1998, *A&A*, 331, L1, doi: [10.48550/arXiv.astro-ph/9801013](https://doi.org/10.48550/arXiv.astro-ph/9801013)
- Siudek, M., Mezcua, M., Circosta, C., et al. 2025, *A&A*, 700, A209, doi: [10.1051/0004-6361/202555463](https://doi.org/10.1051/0004-6361/202555463)
- Son, S., Kim, M., & Ho, L. C. 2022, *ApJ*, 927, 107, doi: [10.3847/1538-4357/ac4dfc](https://doi.org/10.3847/1538-4357/ac4dfc)
- Son, S., Kim, M., & Ho, L. C. 2023, *ApJ*, 958, 135, doi: [10.3847/1538-4357/ad01bc](https://doi.org/10.3847/1538-4357/ad01bc)
- Son, S., Kim, M., & Ho, L. C. 2025, *A&A*, 695, A268, doi: [10.1051/0004-6361/202452467](https://doi.org/10.1051/0004-6361/202452467)
- Son, S., Kim, M., & Ho, L. C. 2026, *A&A*, 706, A122, doi: [10.1051/0004-6361/202557499](https://doi.org/10.1051/0004-6361/202557499)
- Stern, D., Eisenhardt, P., Gorjian, V., et al. 2005, *ApJ*, 631, 163, doi: [10.1086/432523](https://doi.org/10.1086/432523)
- Stern, D., Assef, R. J., Benford, D. J., et al. 2012, *ApJ*, 753, 30, doi: [10.1088/0004-637X/753/1/30](https://doi.org/10.1088/0004-637X/753/1/30)
- Stone, N. C., & Metzger, B. D. 2016, *MNRAS*, 455, 859, doi: [10.1093/mnras/stv2281](https://doi.org/10.1093/mnras/stv2281)
- Szalai, T., Zsíros, S., Fox, O. D., Pejcha, O., & Müller, T. 2019, *ApJS*, 241, 38, doi: [10.3847/1538-4365/ab10df](https://doi.org/10.3847/1538-4365/ab10df)
- Treister, E., & Urry, C. M. 2006, *ApJL*, 652, L79, doi: [10.1086/510237](https://doi.org/10.1086/510237)
- Veilleux, S., & Osterbrock, D. E. 1987, *ApJS*, 63, 295, doi: [10.1086/191166](https://doi.org/10.1086/191166)

- Venanzi, M., Hönl, S., & Williamson, D. 2020, *ApJ*, 900, 174, doi: [10.3847/1538-4357/aba89f](https://doi.org/10.3847/1538-4357/aba89f)
- Virtanen, P., Gommers, R., Oliphant, T. E., et al. 2020, *Nature Methods*, 17, 261, doi: [10.1038/s41592-019-0686-2](https://doi.org/10.1038/s41592-019-0686-2)
- Wada, K. 2012, *ApJ*, 758, 66, doi: [10.1088/0004-637X/758/1/66](https://doi.org/10.1088/0004-637X/758/1/66)
- WISE Team. 2020a, AllWISE Multiepoch Photometry Table, IPAC, doi: [10.26131/IRSA134](https://doi.org/10.26131/IRSA134)
- WISE Team. 2020b, NEOWISE 2-Band Post-Cryo Single Exposure (L1b) Source Table, IPAC, doi: [10.26131/IRSA124](https://doi.org/10.26131/IRSA124)
- Wright, E. L., Eisenhardt, P. R. M., Mainzer, A. K., et al. 2010, *AJ*, 140, 1868, doi: [10.1088/0004-6256/140/6/1868](https://doi.org/10.1088/0004-6256/140/6/1868)
- Yuk, H., Dai, X., Jayasinghe, T., et al. 2022, *ApJ*, 930, 110, doi: [10.3847/1538-4357/ac6423](https://doi.org/10.3847/1538-4357/ac6423)
- Zhuang, M.-Y., & Ho, L. C. 2023, *Nature Astronomy*, 7, 1376, doi: [10.1038/s41550-023-02051-4](https://doi.org/10.1038/s41550-023-02051-4)

APPENDIX

A. EXAMPLE LIGHT CURVES OF ‘SUSPICIOUS’ SOURCE

Figure A1 presents example light curves for the suspicious sources with P_{var} values ranging from 0.95 to 0.99.

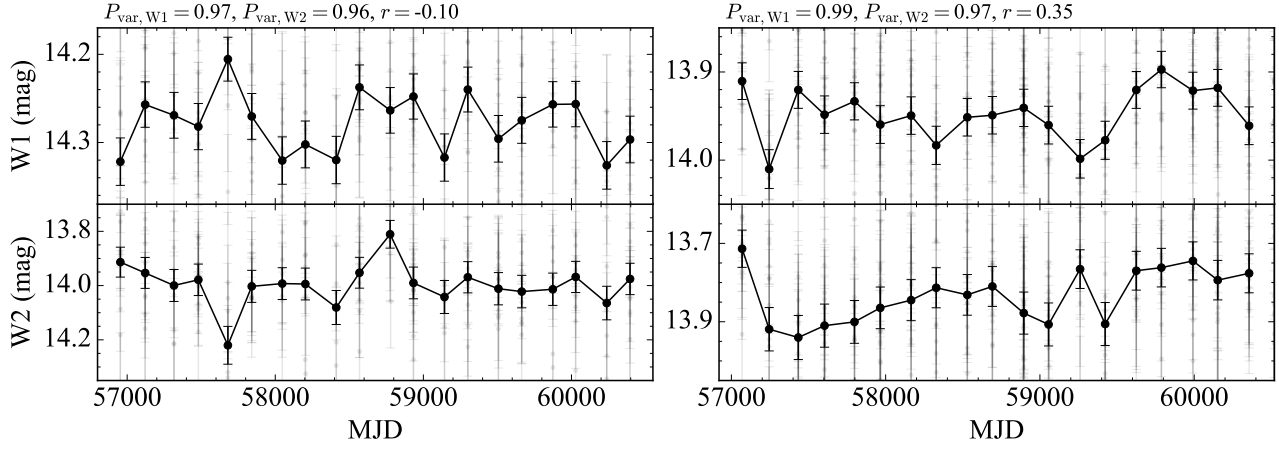


Figure A1. Same as Figure 1, but for suspicious sources with $0.95 < P_{\text{var}} < 0.99$.